ELSEVIER

Journal of Neuroscience Methods 101 (2000) 59–67

JOURNAL OF NEUROSCIENCE METHODS

www.elsevier.com/locate/jneumeth

Tracking of flying insects using pan-tilt cameras

S.N. Fry[a], M. Bichsel[b], P. Müller[a], D. Robert[a,*]

[a] *Zoologisches Institut, University of Zürich, Winterthurerstrasse 190, CH-8057 Zurich, Switzerland*
[b] *Institut für Konstruktion und Bauweisen, ETH-Zentrum, Swiss Institute of Technology, Tannenstrasse 3/CLA, CH-8092 Zurich, Switzerland*

Received 31 March 2000; received in revised form 25 May 2000; accepted 30 May 2000

Abstract

Potent and affordable video and computer systems for automatic data acquisition are becoming increasingly important in behavioural neuroscience. It has remained challenging, however, to acquire data from small and fast-moving animals, such as insects in flight, due to the limited spatial and temporal resolution of the systems currently available. Our research on free-flying insects motivated the development of new methods in the context of two different experimental settings. First, the position and precise body axis direction of honey bees approaching a food source were automatically measured. Second, the flight trajectories of a phonotactic parasitoid fly homing in on its cricket host were recorded in 3D. We used pan-tilt cameras, i.e. cameras with moveable optics, to follow the animal's path with a close up image. Novel methods were developed for image acquisition and position measurement using pan-tilt cameras, as well as calibration and data evaluation in 3D world coordinates. The innovations of this system comprise: (1) Acquisition of images in high spatial detail over large observation areas. (2) Image acquisition at a field rate of 50 Hz PAL. (3) Free positioning of the cameras for 3D acquisition. (4) Computation of the flight path in 3D world coordinates. We illustrate the capabilities of the system with data obtained from a calibration object as well as from the behaviour of unrestricted, free-flying flies and bees. Potential applications in behavioural neuroscience and the psychophysics of sensory perception are briefly discussed.

Keywords: 2D; 3D; Honey bee; Fly; Behaviour; Flight trajectory

1. Introduction

Recent advances in computer technology have stimulated the use of automatic data acquisition systems based on video techniques. In behavioural neurosciences in particular, such developments have been timely, generating new opportunities for the design of more sophisticated behavioural assays. A variety of technical solutions for the automatic acquisition of flight paths (tracking systems) have been developed to fulfil the requirements of the specific experimental task (e.g. Budenberg, 1994; Hoy et al., 1996). Limitations in the hardware and the speed of computation have however forced developers to concede certain technical compromises. Consequently, the proposed solutions tended to be optimised for the specific task and were not readily applicable in different experimental context.

One such limitation is the spatial resolution of the system, which constrains the number of pixels sampling a given area. The experimenter is thus faced with a trade-off between resolution and field of view. A high image detail is beneficial for reliable object detection and at the same time allows additional image analysis to be performed, such as the measurement of the body axis orientation. Lower temporal and spatial resolution can be tolerated if the experimental subject is relatively slow and large compared to the area observed. Conversely, small and fast-moving animals, such as flying insects, cover large distances relative to their body size in a short time. Here, the detail vs. area trade-off causes severe experimental limitations. The use of hardware with exceptionally high spatial resolution yields little improvement and has the disadvantage of higher expenses for the hardware (camera, frame grabber) and higher demand for processing time, which in turn is extremely precious when fast-moving animals need to be tracked.

* Corresponding author. Tel.: +41-1-6354834; fax: +41-1-6355716.
E-mail addresses: snfry@zool.unizh.ch (S.N. Fry), drobert@zool.unizh.ch (D. Robert).

0165-0270/00/$ - see front matter
PII: S0165-0270(00)00253-3

Tracking flying insects is even more challenging if path analysis in a three-dimensional space is envisaged. Obtaining depth information requires two different projections of the object, which can be achieved by using two cameras (Bülthoff et al., 1980; Rayner and Aldridge, 1985; Takken et al., 1996). This approach first necessitates the images from the two cameras to be synchronised, e.g. by external hardware (Dahmen and Zeil, 1984). Second, the cameras typically need to be positioned at right angles, imposing some constraints to the design of the experimental set-up. Third, on line sampling of two images requires considerable computational power. The latter problem can be avoided by processing the data off-line (Voss and Zeil, 1995), with the disadvantages of the need for additional hardware for recording the data, methods for the synchronisation of the images, as well as the additional work required. As an alternative to the use of two cameras, different means of obtaining two projections of an object within a single image were found. One such ingenious system used the object's shadow as the second projection (Voss and Zeil, 1995), whereas other systems used a tilted mirror (Bülthoff et al., 1980; Wehrhahn et al., 1982; Chrásková et al., 1999).

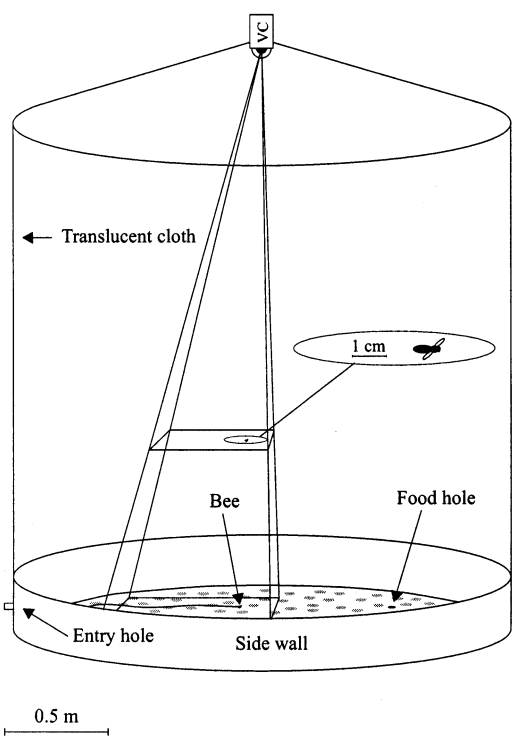

Fig. 1. Flight chamber used in the experiments with honey bees. Bees were trained to enter the flight chamber through the entry hole and fly to a hole in the floor leading to a feeding chamber (not shown). A pan-tilt video camera (VC) protruded through a hole in the roofing and was used to track the bees' flights. The inside of the flight chamber was white, except for pink paper discs scattered on the floor. In some experiments landmarks, covered with white tops, were placed inside the flight chamber. Illumination was from lamps shining onto the translucent cloth from outside the flight chamber. The diameter of the chamber was 2.4 m. The camera was located 2.8 m above the floor. The length of the scale bar is 0.5 m.

Taken together, it remains a challenging task to perform path analysis on small and fast-moving animals in 2D and 3D. The methods described in this report provide new possiblities for powerful and yet practicable path acquisition.

2. Tracking small objects — problems and aims

Free-flying insects were tracked in two different experimental set-ups: in the first experiment, the position and body axis direction of honey bees (*Apis mellifera*) were to be measured in 2D (Fry, 1999; Fry and Wehner, 1999). The bees were trained to enter a large flight chamber and fly to a feeder (Fig. 1). The maximal distance to be tracked was 2.4 m. The critical factor for the measurement of the body axis direction was the number of pixels representing the bee's long axis. The theoretical upper limit for the maximum resolution of the object can be calculated from the resolution of the hardware, the object's size and the observable area. Here, one-dimensional parameters were considered to be the limiting factors and thus the horizontal resolution of the image (r_H), object length (l_{Obj}) and the horizontal length of the area observed (l_{HCam}) were used. The theoretical upper limit for the number of pixels representing the body length (n_H) can be calculated as:

$$n_H = r_H l_{Obj}/l_{HCam}$$

With a typical value for a frame grabber of $r_H = 768$ pixels, $l_{Obj} = 1.5$ cm and $l_{HCam} = 2.4$ m, n_H amounts to 4.8 pixels. In practice objects subtending such small angles are represented by much fewer pixels and may even be difficult to detect reliably due to the low signal to noise ratio elicited by low contrast objects. As a rule of thumb at least ten detected pixels are required for a reasonably accurate measurement of the body axis direction. Using standard techniques it would have been far from possible to perform such measurements over the desired area.

The second task consisted of tracking the flight paths of a parasitoid fly (*Ormia ochracea*) in three-dimensional space (Müller and Robert, 1999). This fly of about 8 mm length locates its host acoustically. In order to investigate the phonotactic behaviour, flies were placed singly on a platform within a uniform black flight room illuminated with infrared lamps (Fig. 6). A loudspeaker 2.8 m distant from the platform was used to attract the fly. It's 3D flight path between the starting platform and the loudspeaker was to be recorded automatically. For 3D tracking using two cameras the same principal limitations of object detection apply for each of the cameras as in the case of a

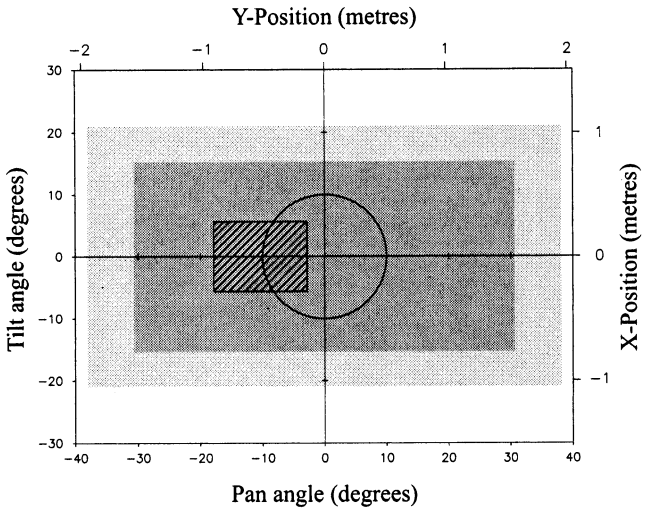

Fig. 2. Field of view of the 2D tracking system. Ordinate: tilt angle. Abscissa: pan angle. Scale at the top and at the right hand side of the figure shows the Cartesian coordinates of the area in the experimental set-up used. Hatched rectangle: image size of the camera at maximum zoom. Dark shaded area: maximum pan and tilt angles of ± 30.6 and 15.3°, respectively. Light shaded area: total area visible by the pan-tilt camera. At maximum deflection angles the object is tracked as long as it remains within the image. The circle shows the path of a calibration object.

single camera, and hence the same reasoning can be applied as in the previous example. In this task reliable object detection was critical and thus the number of pixels (n) representing the object, which can be calculated from the resolution of the image (r), the fly's projected area (a_{Obj}) and the area viewed by the camera (a_{Cam}) as:

$$n = r a_{\mathrm{Obj}} / a_{\mathrm{Cam}}$$

With $r = 768 \times 576$ pixels, $a_{\mathrm{Obj}} = 0.5$ cm^2 and $a_{\mathrm{Cam}} =$ 6 m^2, n amounts to 3.7 pixels. In practice, the fly was barely visible in the image, due to the relatively poor reflectance of the fly and the limited amount of IR illumination. Reliable object detection would have been extremely problematic in such conditions.

The examples show that the use of static optics would have been inappropriate to perform the measurements envisaged by us. The novel concepts implemented in the 'Trackit' system, presented in the following sections, greatly improve on the detectability of small objects.

3. Pan-tilt cameras provide a high virtual resolution over a large area

The trade-off between a high object resolution and a large field of view inherent to video technology is found to be elegantly solved by the visual system of most vertebrates; by directing the gaze to a region of interest, a small part of the visual field is inspected acutely. Similarly to our eyes following an object, we used pan-tilt cameras to follow the insect's flight path.

Pan-tilt cameras are commonly used for surveillance purposes. The optics of a pan-tilt camera are controlled via a serial interface to move in the horizontal (pan) and vertical (tilt) plane (Fig. 3 A). We used Sony LSX PT1 cameras, featuring a resolution of 768 (H) $\times$ 492 (V) effective pixels, a 3 $\times$ zoom set to the maximum focal length of 13.5 mm, pan and tilt angles of ± 30.6 and 15.3°, respectively, and most importantly a very high maximum angular speed of 150°/s.

The advantage of using pan-tilt cameras for the experiments with honey bees is illustrated in Fig. 2. Only a small part of the total area is sampled at one time. The hatched rectangle shows the camera's field of view when pointing at a position of $x = -10°$, $y = 0°$. The maximum range of pan and tilt angles (± 30.6 and 15.3°, respectively) are shown as a dark-shaded rectangle. An object outside this area is tracked as long as it remains within the boundaries of the camera's image. Thus, it is possible to track an object within the limits of the pan and tilt angles plus half the image width and height, respectively (Fig. 2, light-shaded rectangle).

In the set up used for the experiments with honey bees the angle values corresponded to the Cartesian coordinates shown on the top and right hand axis of the figure.

4. Computation of the object's position

The following steps describe the methods developed to calculate the polar coordinates of the object (hereafter referred to as the object direction, $\mathbf{d}_{\mathrm{Obj}}$) relative to the camera body and the steering commands required to keep the moving object close to the image centre. Also refer to Fig. 3B for a schematic of the transformations involved.

Prior to measuring the animal's position, it is necessary to determine the camera-dependent parameters in a calibration procedure. The camera calibration provides the mapping of steering commands to camera movements specific for the camera used, as well as a mapping of the object's position in the image to the camera-head centred object direction (calibration factors f_x and f_y and the offsets x_0 and y_0, used in step 4. For each image acquired the following calculations are performed:

4.1. Step 1

Current pan and tilt angles from steering commands. The current pan (α) and tilt (β) angles of the camera are computed on line from the history of steering commands sent to the camera, based on the camera-

specific mapping of steering commands to camera movements obtained from the camera calibration.

4.2. Step 2

Rotation matrix for camera-head centred coordinates to camera-body centred coordinates. The current pan (α) and tilt (β) angles are be combined into the rotation matrix $\mathbf{M}_{\mathrm{RotHB}}$ that transforms camera-head centred coordinates into camera-body centred coordinates. With a zero-viewing direction of the camera defined as (0, 0, 1), the matrix can be calculated as:

$$\mathbf{M}_{\mathrm{RotHB}} = \begin{pmatrix} \cos\alpha & 0 & \sin\alpha \\ 0 & 1 & 0 \\ -\sin\alpha & 0 & \cos\alpha \end{pmatrix} \begin{pmatrix} 1 & 0 & 0 \\ 0 & \cos\beta & -\sin\beta \\ 0 & \sin\beta & \cos\beta \end{pmatrix}$$

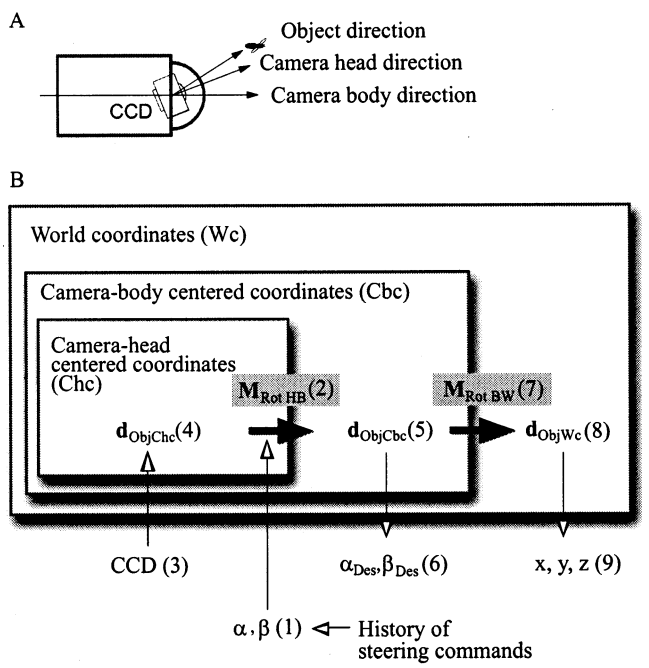

Fig. 3. Pan-tilt camera and schematic of calculations performed for tracking. (A) Top view of a pan-tilt camera with panned optics. The bottom arrow shows the orientation of the camera body, the middle arrow the orientation of the camera head, including the optics and the CCD chip. The top arrow shows the viewing direction to the object. (B) Calculations performed during the tracking process. Object directions in camera-head centred coordinates ($\mathbf{d}_{\mathrm{ObjChc}}$) are converted into camera-body centred coordinates ($\mathbf{d}_{\mathrm{ObjCbc}}$) by applying rotation matrix $\mathbf{M}_{\mathrm{RotHB}}$, and finally, in the case of 3D tracking, into world coordinates ($\mathbf{d}_{\mathrm{ObjWc}}$) by applying rotation matrix $\mathbf{M}_{\mathrm{RotBW}}$. The object direction in camera-body centred coordinates ($\mathbf{d}_{\mathrm{ObjCbc}}$) is used to compute the desired pan (α) and tilt (β) angles, which are sent to the camera as a steering command. The history of steering commands sent are in turn used to calculate the present pan and tilt angles of the camera and the rotation matrix $\mathbf{M}_{\mathrm{RotHB}}$. The process is repeated at field rate (50 Hz PAL) with the acquisition of the image from the CCD chip.

4.3. Step 3

Object detection, position in the image and body axis direction analysis. The object's position in the image in pixels (x, y) is calculated with sub-pixel accuracy as the centre of gravity of the image points within the detected object contour. Object detection is based on the contrast, with a variable intensity threshold set by the user. Dark objects are detected against a bright background or vice versa. Furthermore, the orientation of the object's long axis is determined and stored as the sine and the cosine of the measured body axis direction, modulo 180°. Thus 'front' and 'back' are not distinguished by the system. This ambiguity can subsequently be resolved by considering the direction of flight and the image sequence.

4.4. Step 4

Object direction in camera-head centred coordinates. From the position of the object in the image, object direction in a camera-head centred coordinate system ($\mathbf{d}_{\mathrm{ObjChc}}$) can be calculated using the calibration factors f_x and f_y and the offsets x_0 and y_0 obtained from the camera calibration procedure as:

$$\mathbf{d}_{\mathrm{ObjChc}} = \begin{pmatrix} f_x(x - x_0) \\ f_y(y - y_0) \\ 1 \end{pmatrix}$$

f_x and f_y are determined by the chosen focal length and the physical pixel size on the CCD chip, x_0 and y_0 are determined by the CCD chip's exact position in the optical path.

4.5. Step 5

Object direction in camera-body centred coordinates. The measured camera-head centred coordinates ($\mathbf{d}_{\mathrm{ObjChc}}$) obtained in step 5 can be combined with the rotation matrix $\mathbf{M}_{\mathrm{RotHB}}$ obtained in step 2 to calculate the object direction in a camera-body centred coordinate system ($\mathbf{d}_{\mathrm{ObjCbc}}$):

$$\mathbf{d}_{\mathrm{ObjCbc}} = \mathbf{M}_{\mathrm{RotHB}}\mathbf{d}_{\mathrm{ObjChc}}$$

In the case of a single camera used for tracking in two dimensions, these data are stored immediately after termination of tracking. In the case of 3D tracking, the data are obtained from each camera and processed further (6.3).

4.6. Step 6

Calculation of steering commands. To keep the image of the object near the image centre, the desired viewing direction of the camera ($\mathbf{d}_{\mathrm{DesObjCbc}}$) needs to be

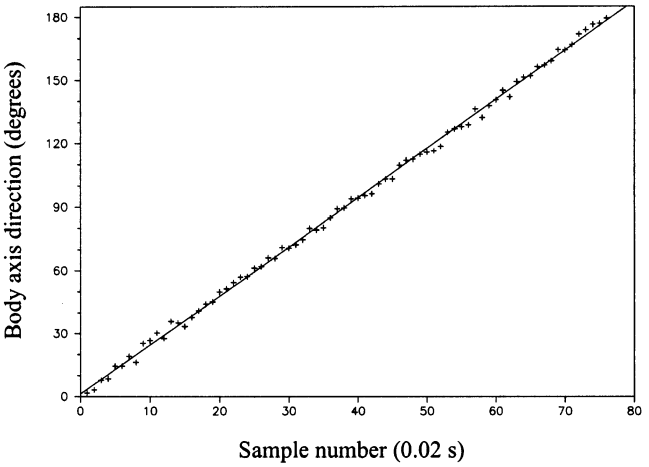

Fig. 4. Body axis direction measured for a dried bee rotated through 180° on a circular path of 1 m diameter and at a speed of about 1 m/s. The data were sampled at intervals of 20 ms.

Table 1
Percentiles of the error distributions of the data shown in Figs. 5A and 7A[a]

Dimension	Percentiles		
	5	50	95
Fig. 5 *(°)*			
X	−0.06	0.09	0.23
Y	−0.24	−0.05	0.06
Fig. 7 *(m)*			
X	−0.029	−0.020	0.002
Y	−0.033	0.003	0.042
Z	−0.024	0.012	0.036

[a] Note that units are degrees and metres for the data of Figs. 5A and 7A, respectively.

determined. The system strives to keep the object as close to the image centre as possible, such that ideally $\mathbf{d}_{\mathrm{DesObjCbc}} = \mathbf{d}_{\mathrm{ObjCbc}}$. During tracking the values differ due to the time lag of the system. The pan and tilt angles (α_{Des} and β_{Des}, respectively) to be sent as steering commands to the camera can be calculated from the current object direction obtained in step 5 as:

$$\alpha_{\mathrm{Des}} = -\operatorname{atan}2(x_{\mathrm{ObjCbc}}, z_{\mathrm{ObjCbc}})$$

$$\beta_{\mathrm{Des}} = \operatorname{atan}2(y_{\mathrm{ObjCbc}}, z_{\mathrm{ObjCbc}}/\cos(\alpha_{\mathrm{Des}}))$$

with

$$\mathbf{d}_{\mathrm{ObjCbc}} = \begin{pmatrix} x_{\mathrm{ObjCbc}} \\ y_{\mathrm{ObjCbc}} \\ z_{\mathrm{ObjCbc}} \end{pmatrix}$$

The speed and precision with which the camera follows the object is critical if the object is to remain within the image. A high sampling rate is especially important for keeping the object in the image by reducing the reaction time of the system. To allow reliable tracking of fast-moving objects, the fields (i.e. the interlaced half-frames of the images) were sampled at 50 Hz (PAL). Typically, automatic image analysis systems do not go beyond the temporal resolution of the frame rate of the video hardware, i.e. 25 Hz (PAL) or 30 Hz (NTSC). Thus the sampling rate was doubled while using standard hardware.

5. Tracking in 2D

5.1. Calibration of 2D world coordinates

As described in the previous section, the tracking system provides us with the object direction relative to the camera body ($\mathbf{d}_{\mathrm{ObjCbc}}$). For the analysis of behavioural data, it is often more convenient to transform the polar coordinates into an external reference system using Cartesian coordinates. If the movements of the animal lie in or close to a plane, as was the case with the honey bees, it is possible to calculate the approximate position of the bee in world coordinates. In principle, this could be done by geometric calculations based on the measured angles and the camera's position (with six degrees of freedom). A simpler and more robust method was applied by measuring a number of defined positions in the plane and arbitrarily fitting a function to the measured data. As the angles measured were relatively small, a linear function was used as an approximation. The Cartesian coordinates obtained this way are shown on the top and right hand axis in Fig. 2.

5.2. Measurements with an artificial stimulus

To determine the accuracy of the position and the body axis direction measurements, a dried specimen of a honey bee was placed on a carrousel (Fig. 2) located in the flight chamber under typical experimental conditions. In this way data of a circular path of 1 m diameter and a speed of around 1 m/s were acquired, in the range of the typical flight speeds of the bees observed in the experiments. Fig. 4 shows the measured body axis direction of a 180° rotation on the carrousel as a function of the field number (corresponding to 20-ms intervals). Under perfect conditions a linear change in body axis direction is expected. A linear regression performed on the data yielded a Pearson linear correlation coefficient of 0.9993.

The measured object positions are shown separately for the x and y dimensions in Fig. 5A. The lines show the best fit of a circle to a data fraction corresponding to a 360° rotation. The measurements lay close to the expected circular path (Fig. 5A, inset), satisfying the

requirements for the accuracy of our behavioural analyses.

5.3. Tracking honey bees in free flight

The flights of honey bees were recorded in a uniform white flight chamber (Fig. 1). The bees contrasted well against the lighter background. To enable the bees to perform flight stabilisation, pink discs were scattered on the floor. Pink was used because honey bees do not possess a red receptor and therefore the discs provided a higher intensity contrast to the bees than to the camera system.

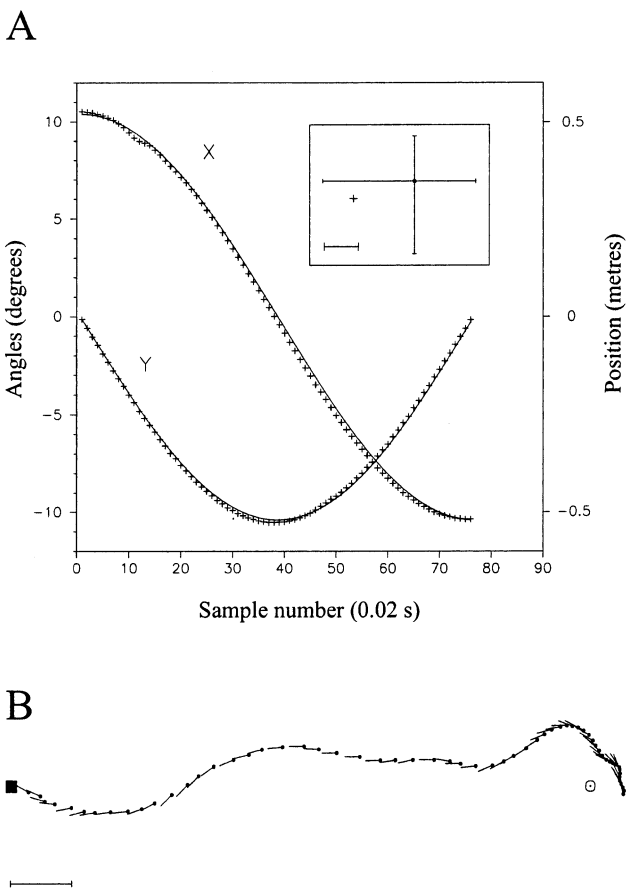

Fig. 5. Position of a calibration object and flight path of a bee. (A) Position of a dried bee rotated on a circular path. The same sample of data was used as for Fig. 4. Ordinate: position in degrees in a camera-body centred frame of reference. Abscissa: frame number, corresponding to 20 ms. Fitted values are shown by the solid lines. The inset shows the median and the 95-percentiles of the residuals. The zero position is marked by the cross. The length of the scale bar is 0.1°. The statistics are listed in Table 1. (B) Flight path of a honey bee. The dot-and-line symbols indicate the position and body axis direction of every second data point, corresponding to intervals of 40 ms. The bee took off from a platform (black square on the left of the figure), flew towards a hole in the floor board (symbolised by the dot and circle) and landed close to it. The distance from starting platform to the hole was 1.9 m. The length of the scale bar is 0.1 m.

At the beginning of each trial the camera was automatically pointed in the pre-defined direction of the entry hole. As soon as a bee entered the flight chamber it was detected and followed by the camera. After the bee had left the flight chamber through the food hole, tracking was automatically terminated and the bee's positions were stored. Fig. 5B depicts the position andbody axis direction of a typical flight of a honey bee flying a distance of 2.0 m from a starting platform to a position close to the food hole. The dot-and-line symbols show the positions and body axis directions of every second data sample. The intermediate points are not shown for reasons of clarity. The bees' flights were tracked very reliably and the body axis measurements appeared realistically continuous.

6. Tracking in 3D

6.1. 'Synchronisation' of the images

The use of two cameras necessitates the coordination of image acquisition, e.g. by triggering the image acquisition of both cameras using external hardware (Dahmen and Zeil, 1984). This method was not applicable to the camera type used, however, and therefore a method was developed to virtually synchronise the cameras using software methods. Let us assume two fields were acquired at times t_1 and t_2, in which the object positions x_1, y_1 and x_2, y_2, respectively, were determined. By linear interpolation of the position in time it is possible to estimate the position of the object in the image at time t as:

$$x_t = (t - t_1)(x_2 - x_1)/(t_2 - t_1),$$

and

$$y_t = (t - t_1)(y_2 - y_1)/(t_2 - t_1)$$

In the worst case, the fields are acquired with a phase shift of 180°, which results in a time lag of 1/100 s. The error resulting from the interpolation is the non-linear change of position during this time, which can be assumed to be negligible. The software method has the advantage that any type of camera can be used and that no external synchronisation hardware is required.

6.2. Calibration of the 3D world coordinate space

To obtain the fly's flight trajectory in 3D, two pan-tilt cameras are positioned appropriately to obtain different projections of the fly's position. To compute world coordinates, the current locations of each camera and their orientations need to be known (i.e. six degrees of freedom for each camera). This measurement is performed in a calibration procedure before beginning the measurements. We used a calibration cube (side

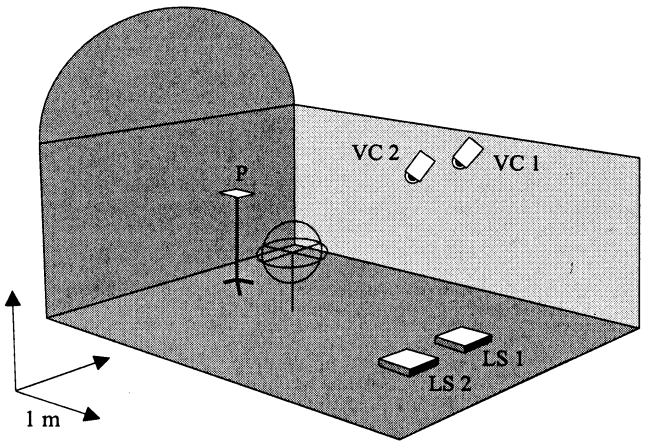

Fig. 6. Flight chamber used in the experiments with flies. The side walls and the roofing are made of gauze and the floor and parts of the side walls are covered with black fabric. Infra-red lamps illuminate the flight chamber from above. Flies are placed on a platform (P). A loudspeaker (LS) is used to emit the sound of a cricket to attract the fly. Two infra red sensitive pan-tilt video cameras (VC) protrude into the flight chamber from above. Scale bars are 1 m.

length: 1 m) with eight small, dimly lit 12-V light bulbs positioned at its corners as a frame of reference. The object directions $\mathbf{d}_{\mathrm{ObjCbc1}}$ and $\mathbf{d}_{\mathrm{ObjCbc2}}$ of every corner of the cube are measured by each camera. An algorithm is applied to compute the locations and orientations of the cameras for which the squared deviation between the predicted and measured viewing directions are minimal. The algorithm solves a non-linear optimisation problem using a steepest descent method (Press, 1994). The measurements of the calibration points were performed using the program's user interface. The calibration procedure yields the positions of the cameras' optical centres ($\mathbf{p}_1$ and $\mathbf{p}_2$) and their zero-viewing directions.

6.3. Computation of object position in 3D Cartesian coordinates

For the cameras 1 and 2 the object direction in camera-body centred coordinates ($\mathbf{d}_{\mathrm{ObjCbc1}}$ and $\mathbf{d}_{\mathrm{ObjCbc2}}$) are calculated independently, as described in steps 1–6 of Section 4. The following steps (7–9) describe how the data obtained by two cameras is combined to compute the Cartesian coordinates of the object (see Fig. 3 for a flow chart overview).

6.3.1. Step 7

Rotation matrix for camera-body centred coordinates to world coordinates. Based on the 3D calibration data (Section 6.2), the rotation matrices $\mathbf{M}_{\mathrm{RotBW1}}$ and $\mathbf{M}_{\mathrm{RotBW2}}$ are determined for each camera, with which the camera-body centred coordinates are transformed into world coordinates.

6.3.2. Step 8

Object directions in world coordinates. The measured object directions of each camera ($\mathbf{d}_{\mathrm{ObjCbc1}}$ and $\mathbf{d}_{\mathrm{ObjCbc2}}$) are combined with the rotation matrices $\mathbf{M}_{\mathrm{RotBW1}}$ and $\mathbf{M}_{\mathrm{RotBW2}}$, respectively, to obtain the object directions for each camera in world coordinates ($\mathbf{d}_{\mathrm{ObjWc1}}$ and $\mathbf{d}_{\mathrm{ObjWc2}}$) as:

$$\mathbf{d}_{\mathrm{ObjWc1}} = \mathbf{M}_{\mathrm{RotBW1}}\mathbf{d}_{\mathrm{ObjCbc1}}$$

$$\mathbf{d}_{\mathrm{ObjWc2}} = \mathbf{M}_{\mathrm{RotBW2}}\mathbf{d}_{\mathrm{ObjCbc2}}$$

6.3.3. Step 9

3D position in world coordinates. Ideally, the lines of sight of the two cameras intersect at the true 3D location of the object. In practice, however, there are small inaccuracies in the measurement and the lines do not intersect. Therefore an approximation for the position of the object ($\mathbf{o}$) needs to be found. This point can be determined with the shortest distance between the lines of sight $\mathbf{d}_{\mathrm{ObjWc1}}$ and $\mathbf{d}_{\mathrm{ObjWc2}}$ by minimising

$$(\mathbf{p}_1 + a\mathbf{d}_{\mathrm{ObjWc1}} - \mathbf{o})^2 + (\mathbf{p}_2 + b\mathbf{d}_{\mathrm{ObjWc2}} - \mathbf{o})^2$$

with respect to a, b, and $\mathbf{o}$. $\mathbf{p}_1$ and $\mathbf{p}_2$ are the positions of the cameras.

This results in the three equations

$$\mathbf{o} = 1/2(\mathbf{p}_1 + a\mathbf{d}_{\mathrm{ObjWc1}} + \mathbf{p}_2 + b\mathbf{d}_{\mathrm{ObjWc2}})$$

$$a\mathbf{d}_{\mathrm{ObjWc1}}\mathbf{d}_{\mathrm{ObjWc1}} - b\mathbf{d}_{\mathrm{ObjWc1}}\mathbf{d}_{\mathrm{ObjWc2}} = \mathbf{d}_{\mathrm{ObjWc1}}(\mathbf{p}_2 - \mathbf{p}_1)$$

$$-a\mathbf{d}_{\mathrm{ObjWc2}}\mathbf{d}_{\mathrm{ObjWc1}} + b\mathbf{d}_{\mathrm{ObjWc2}}\mathbf{d}_{\mathrm{ObjWc2}} = \mathbf{d}_{\mathrm{ObjWc2}}(\mathbf{p}_1 - \mathbf{p}_2)$$

The parameters a and b are obtained by solving the pair of linear equations in a and b:

$$a = (\mathbf{d}_{\mathrm{ObjWc2}}(\mathbf{p}_2 - \mathbf{p}_1))(\mathbf{d}_{\mathrm{ObjWc1}}\mathbf{d}_{\mathrm{ObjWc2}}) - (\mathbf{d}_{\mathrm{ObjWc1}}(\mathbf{p}_2 - \mathbf{p}_1))(\mathbf{d}_{\mathrm{ObjWc2}}\mathbf{d}_{\mathrm{ObjWc2}})/(\mathbf{d}_{\mathrm{ObjWc1}}\mathbf{d}_{\mathrm{ObjWc1}})(\mathbf{d}_{\mathrm{ObjWc2}}\mathbf{d}_{\mathrm{ObjWc2}}) - (\mathbf{d}_{\mathrm{ObjWc1}}\mathbf{d}_{\mathrm{ObjWc2}}) - \mathbf{d}_{\mathrm{ObjWc1}}\mathbf{d}_{\mathrm{ObjWc2}})$$

$$b = (\mathbf{d}_{\mathrm{ObjWc2}}(\mathbf{p}_2 - \mathbf{p}_1))(\mathbf{d}_{\mathrm{ObjWc1}}\mathbf{d}_{\mathrm{ObjWc1}}) - (\mathbf{d}_{\mathrm{ObjWc1}}(\mathbf{p}_2 - \mathbf{p}_1))(\mathbf{d}_{\mathrm{ObjWc1}}\mathbf{d}_{\mathrm{ObjWc2}})/(\mathbf{d}_{\mathrm{ObjWc1}}\mathbf{d}_{\mathrm{ObjWc1}})(\mathbf{d}_{\mathrm{ObjWc2}}\mathbf{d}_{\mathrm{ObjWc2}}) - (\mathbf{d}_{\mathrm{ObjWc1}}\mathbf{d}_{\mathrm{ObjWc2}}) - \mathbf{d}_{\mathrm{ObjWc1}}\mathbf{d}_{\mathrm{ObjWc2}}).$$

Back-substitution of a and b into $\mathbf{o} = 1/2(\mathbf{p}_1 + a\mathbf{d}_{\mathrm{ObjWc1}} + \mathbf{p}_2 + b\mathbf{d}_{\mathrm{ObjWc2}})$ yields the approximation of the object's position in the Cartesian coordinate frame as defined by the calibration cube, with

$$\mathbf{o} = \begin{pmatrix} x \\ y \\ z \end{pmatrix}$$

The described methods allow the experimenter to freely position the cameras as demanded by the experimental situation. Consequently, 3D tracking becomes more generally applicable with set-ups that cannot easily be modified to accustom for specific camera orientations.

6.4. Measurements with an artificial stimulus

To measure a defined dynamic stimulus a light bulb was placed on a carrousel of 1 m diameter and rotated at a speed of approximately 1 m/s, which was in the typical range of the flight speeds of the flies measured in the experiments (Fig. 6). As before, the data were converted into 3D Cartesian coordinates.

The measured values are shown in Fig. 7A. In all three dimensions, the measured values were sufficiently precise for behavioural analyses. For practical reasons the cameras were separated by only 1 m at typical object distances of around 2 m, which corresponds to a parallax angle of only 28°. The accuracy of the measurement in the viewing direction of the cameras is expected to decrease the smaller the parallax angle between the cameras. Thus, a higher accuracy could be achieved by positioning the cameras orthogonally relative to each other.

6.5. Tracking 3D flight paths of flies

The flies to be tracked were nocturnal parasitoids that can rely exclusively on sound cues to locate their host. To rule out the influence of light, it was essential to provide illumination to the infra-red (IR)-sensitive cameras in a light spectrum invisible to the animals. Under IR light ($\lambda = 875$ nm, TSMA 6503 LED, 25 mW ($I_F = 100$ mA, $t_P = 20$ ms), Temic Semiconductors), the flies appeared bright against the dark background. In order to track a bright object against a dark background (as opposed to the previous example with honey bees) the sensitivity threshold was reversed.

An example flight is shown in Fig. 7B. The fly was placed on a platform, where it rested until it heard the sound of a cricket emitted by a loudspeaker placed on the floor. In the mean time the tracking process was started. When the fly reached the loudspeaker tracking was terminated by the user. The 3D Cartesian flight coordinates were automatically saved on hard disc after termination of the tracking process as a time series in ASCII format.

7. Discussion

Recording the behaviour of animals with sufficient spatial and temporal resolution has constituted a challenge in situations that involve small and fast-moving animals, such as flying insects (Bülthoff et al., 1980; Wehrhahn et al., 1982; Dahmen and Zeil, 1984; Voss and Zeil, 1995; Riley et al., 1996; Takken et al., 1996; Schilstra and van Hateren, 1998). The observational difficulties are inherently linked to the nature of flying insects, as they cover large distances relative to their body size in a short time.

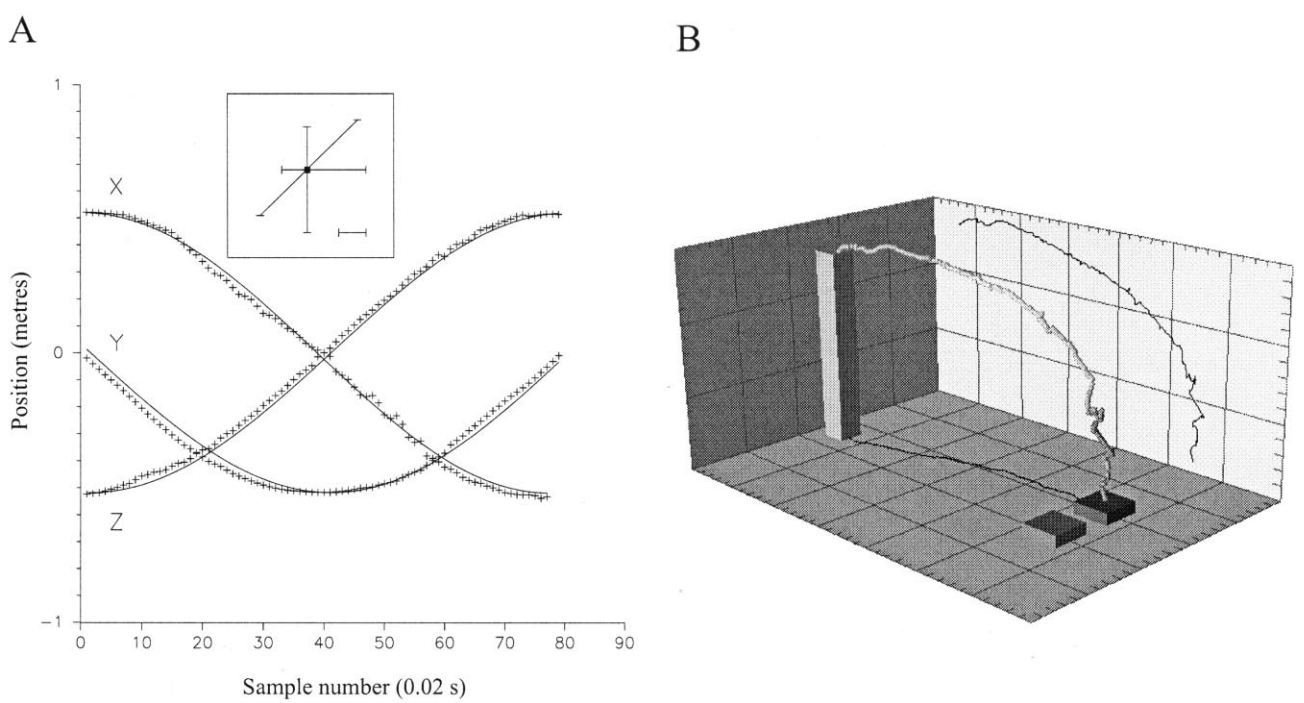

Fig. 7. Position of a calibration object and flight path of a fly. (A) Measured position of a small dimly lit light bulb rotated through 180° in the horizontal (x and y values) and the vertical plane (z values). Ordinate: position in world coordinates (m). Abscissa: frame number, corresponding to 20 ms. The lines show the fitted data. The inset shows the median and the 95-percentiles of the errors, with the y-value shown 1/3 shortened for perspective reasons (also refer to Table 1). (B) Flight performed by the parasitic fly *Ormia ochracea*. Flight direction from the left to the right. The fly was placed on a platform and was attracted to a loudspeaker emitting the sound of it's host cricket.

The method for data acquisition described here permits the quantitative path analysis of unrestrained animals on line, at a temporal and spatial scale adequate for flying insects. These possibilities have manifold implications for experimentation in behavioural neurosciences. Trajectories comprising hundreds of body lengths can be measured and long time-series can be acquired. The experimental design becomes more flexible and gains in relevance towards the natural behavioural context. Furthermore, the high temporal resolution is sufficient to extract important secondary flight parameters, such as flight speed, distance to goal, curvature of the flight trajectory, etc. (Müller and Robert, in preparation).

Further, the use of the present system provides the experimenter with the animal's position at a relatively high temporal resolution. As demonstrated here, the immediate availability of the positional information in space is a prerequisite for the closed-loop control of the cameras's tracking motion. Using this positional information on line, the stimuli delivered can be dynamically modified by the animal as it flies through the exprimental space (Fry et al., in preparation; Müller and Robert, in preparation). This approach is currently applied in our laboratory and provides enticing opportunities to examine the orientation behaviour and the psychophysics of acoustic and visual perception in free-flying insects.

Acknowledgements

We thank Helmut Heise and Hans-Jörg Baumann for technical support, Martin Göpfert for helpful comments on the manuscript and all members of the Robert lab for valuable discussions. We also wish to thank Rüdiger Wehner and Rolf Pfeifer for initial encouragement. The work was supported by the Swiss National Science Foundation, the Claraz Foundation and the Schering Foundation.

References

Budenberg WJ. Video techniques for behavioural data collection. Psychol Software News 1994;5:39–40.

Bülthoff H, Poggio T, Wehrhahn C. 3-D analysis of the flight trajectories of flies (*Drosophila melanogaster*). Z Naturforsch 1980;35c:811–5.

Chrásková J, Kaminsky Y, Krekule I. An automatic 3D tracking system with a PC and a single TV camera. J Neurosci Methods 1999;88:159–200.

Dahmen HJ, Zeil J. Recording and reconstructing 3-dimensional trajectories — a versatile method for the field biologist. Proc R Soc London B 1984;222(1226):107–13.

Fry SN. Goal-navigation in honey bees. University of Zürich, 1999 Ph.D. thesis.

Fry SN, Wehner R. A simple model explains goal-navigation in honey bees. In: Proceedings of the 27th Gött. Neurobiology Conference, vol. II. Stuttgart: Thieme, 1999:428.

Hoy JB, Koehler PG, Patterson RS. A microcomputer-based system for real-time analysis of animal movement. J Neurosci Methods 1996;64:157–61.

Müller P, Robert D. The phonotactic behaviour of the parasitoid fly *Ormia ochracea*. In: Proceedings of the 27th Gött. Neurobiology Conference, vol. I. Stuttgart: Thieme, 1999:81.

Press WH. Numerical Recipes in C: The Art of Scientific Computing. Cambridge: Cambridge University Press, 1994.

Rayner JMV, Aldridge HDJN. Three-dimensional reconstruction of animal flight paths and the turning flight of microchiropteran bats. J Exp Biol 1985;118:247–65.

Riley JR, Smith AD, Reynolds DR, Edwards AS, Osborne JL, Williams IH, Carreck NL, Poppy GM. Tracking bees with harmonic radar. Nature 1996;379(6560):29–30.

Schilstra C, van Hateren JH. Using miniature sensor coils for simultaneous measurement of orientation and position of small, fast-moving animals. J Neurosci Methods 1998;83:125–31.

Takken W, Huisman PWT, Buma MOS, Noldus LPJJ. Three-dimensional video tracking and analysis of the flight of nocturnal anopheline mosquitoes. In: Measuring Behavior '96, Utrecht, 1996:104–5.

Voss R, Zeil J. Automatic tracking of complex objects under natural conditions. Biol Cybern 1995;73:415–23.

Wehrhahn C, Poggio T, Bülthoff H. Tracking and chasing in houseflies (*Musca*). Biol Cybern 1982;45:123–30.